# BiCoRE: Combining a PERC-type cell process with n-type wafers

**Thorsten Dullweber**, **Nadine Wehmeier**, **Anja Nowack**, **Till Brendemühl**, **S. Kajari-Schröder** & **R. Brendel**,
Institute for Solar Energy Research Hamelin (ISFH), Emmerthal, Germany

## ABSTRACT

The p-type monofacial passivated emitter and rear cell (PERC) is currently entering into mass production, but the efficiency of this type of cell is affected by light-induced degradation (LID). A novel solar cell design is introduced here – BiCoRE, which is an acronym for 'bifacial co-diffused rear emitter'. The BiCoRE cell process is almost identical to the PERC process sequence with a proven high-volume capability, but uses LID-stable n-type wafers instead. A plasma-deposited boron silicate glass (BSG) silicon nitride ($SiN_z$) stack at the rear side of the BiCoRE cells acts as a protection layer against texturing and $POCl_3$ diffusion and as a boron dopant source during the $POCl_3$ co-diffusion, as well as a passivation layer. The rear contacts are formed by laser contact opening (LCO) and by screen printing an Al finger grid, similar to the method used for the recently introduced bifacial PERC+ solar cells. The Al finger grid allows bifaciality and enables conversion efficiencies of up to 21.1% to be obtained with n-type reference solar cells. The multifunctional BSG/$SiN_z$ stack demonstrates conversion efficiencies of up to 20.6% with BiCoRE solar cells. When illuminated from the rear side, the BiCoRE cells yield conversion efficiencies of up to 16.1%, which corresponds to a bifaciality of 78%.

## Introduction

Several leading solar cell manufacturers, such as SolarWorld, Hanwha Q-Cells, Trina Solar and others [1–5], are beginning to launch mass production of passivated emitter and rear cells (PERCs). The ITRPV photovoltaic technology roadmap forecasts a market share for PERC solar cells of 35% by 2019 [6]. These industrial PERC cells utilize p-type wafers and a full-area screen-printed aluminium (Al) rear layer that only locally contacts the silicon wafer in regions where the rear passivation has been removed by laser contact opening (LCO). The full-area aluminium layer consumes a high quantity of Al paste, of 1.0 to 1.5g per wafer, and prevents any transmission of sunlight from the rear side to the silicon wafer, thus ruling out any bifacial applications of these industrial PERC cells.

A bifacial PERC solar cell, called *PERC+*, was recently introduced [7], in which a screen-printed Al finger grid was implemented instead of the full-area Al layer. The resulting PERC+ cells demonstrate front-side efficiencies of up to 21.5% (which are comparable to those achieved by monofacial PERC cells) and rear-side efficiencies of up to 16.7% [8]. The application of bifacial modules in PV power plants may increase the energy yield by up to 20% in comparison to monofacial modules, depending on the specific installation conditions [7,9,10]. Accordingly, the ITRPV roadmap predicts a market share for bifacial solar cell technologies of 15% by 2019 [6]. In addition, the bifacial PERC+ solar cells show deeper Al-BSFs and a reduced number of voids in the local Al rear contacts [7], since the Al fingers change the Al-Si alloying process because of the limited aluminium volume [11].

The last few years have seen the development of industrial passivated emitter and rear totally diffused (PERT) solar cells; these use n-type wafers and entail boron doping of the rear wafer side, forming a so-called *back junction (BJ)* [12–15]. The manufacturing sequence for n-type PERT BJ cells is very similar to that for p-type PERC cells, requiring only a few modifications, such as the integration of the rear boron doping as well as wider LCOs of the rear passivation layer [14]. Consequently, n-PERT BJ cells may become an attractive option for p-PERC solar cell manufacturers in migrating their production process from p-type wafers to n-type wafers for as long as light-induced degradation (LID) remains a limiting factor of the conversion efficiency of p-PERC cells [16,17], despite recent advances in developing industrial regeneration processes [18,19].

As in the case of p-PERC cells, n-PERT BJ cells typically employ a full-area Al rear layer and are thus monofacial. In order to simplify the process flow of n-PERT BJ cells, it has been demonstrated that the rear-side boron doping can be realized by depositing a boron silicate glass (BSG) layer using plasma-enhanced chemical vapour deposition (PECVD), and capping this with a $SiN_z$ layer, which is then exposed to a $POCl_3$ co-diffusion [20–23]. The BSG/$SiN_z$ stack acts as a diffusion barrier against phosphorus, whereas during the $POCl_3$ co-diffusion the boron diffuses from the BSG into the silicon wafer. To date, n-PERT BJ cell efficiencies of up to 21.0% have been demonstrated using this technique [24]. A promising approach to further simplify the process sequence is to use the BSG/$SiN_z$ stack also as a passivation layer [25,26] instead of removing it after co-diffusion and applying an $AlO_x/SiN_y$ passivation. Preliminary results based on test wafers report emitter saturation current densities of around 50fA/cm$^2$ with a BSG/$SiN_z$ stack as the doping source and passivation layer [25], and conversion efficiencies of up to 19.8% [26] for n-PERT front-junction cells.

> "The first BiCoRE cells have demonstrated efficiencies of up to 20.6% and bifacialities of 78%."

Bifacial n-PERT BJ cells with a screen-printed Al finger grid on the rear side instead of a full-area Al rear layer were recently demonstrated for the first time [27]. Additionally, these cells employed a PECVD BSG/$SiN_z$ stack as a boron dopant source and as a rear passivation layer using a very lean process sequence. This novel industrial solar cell design has been named *BiCoRE*, which stands

| n-PERT BJ | BiCoRE | PERC+ |
|---|---|---|
| Cleaning | Cleaning | Cleaning |
| $BBr_3$ diffusion | | |
| BSG etch | | |
| Rear: SiNz | Rear: $BSG/SiN_z$ | |
| Texturing | Texturing | Texturing |
| $POCl_3$ diffusion | $POCl_3$ co-diffusion | $POCl_3$ diffusion |
| PSG etch | PSG etch | Polishing/PSG |
| Rear: $AlO_x/SiN_y$ | | Rear: $AlO_x/SiN_y$ |
| Front: $SiN_y$ | Front: $SiN_y$ | Front: $SiN_x$ |
| Laser ablation | Laser ablation | Laser ablation |
| Ag screen printing | Ag screen printing | Ag screen printing |
| Al screen printing | Al screen printing | Al screen printing |
| Firing | Firing | Firing |
| **13** process steps | **10** process steps | **10** process steps |

**Table 1. Process sequences for various cell types. The n-PERT BJ cells utilize $BBr_3$ and $POCl_3$ as doping sources and $AlO_x/SiN_y$ as rear passivation, with the same process sequence being used for both monofacial and bifacial cells. In the case of the bifacial n-type BiCoRE cells, a PECVD $BSG/SiN_z$ layer is utilized as the protection layer, boron doping source and passivation layer. For comparison, a typical process flow for p-type PERC+ cells is also shown.**

for 'bifacial co-diffused rear emitter' [27]. The first BiCoRE cells have demonstrated efficiencies of up to 20.6% and bifacialities of 78% [27,28]. This paper summarizes the features of the novel BiCoRE solar cell.

## Bifacial n-PERT BJ solar cells with rear Al finger grid

First, the use of an Al finger grid as the rear contact of n-PERT BJ cells will be evaluated and optimized. For this, an n-PERT BJ reference process with separate $BBr_3$ and $POCl_3$ diffusions and employing $AlO_x/SiN_y$ as rear passivation will be used. The process sequence is shown in Table 1, column 1, and is described in detail in Lim et al. [29].

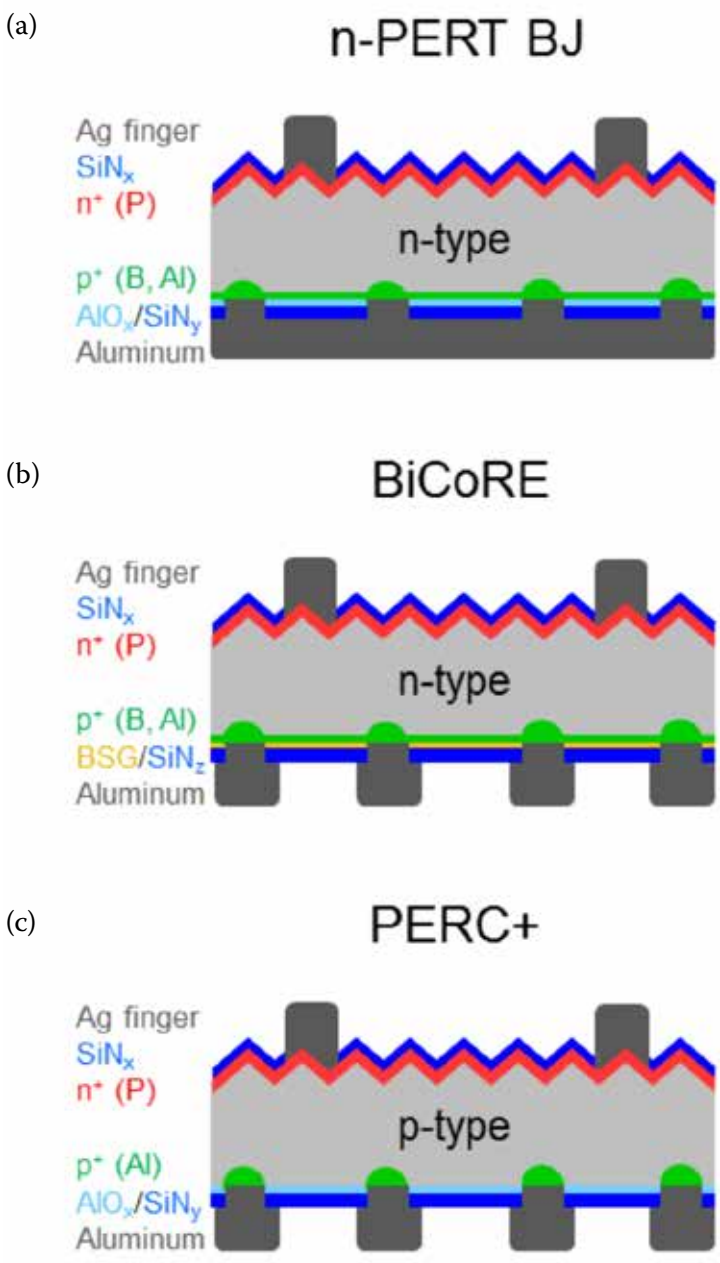


**Figure 1. Schematic diagrams of (a) n-PERT BJ, (b) BiCoRE and (c) PERC+ solar cells resulting from the process flows given in Table 1. The n-PERT BJ cell is processed as a monofacial cell with a full-area Al layer (as shown in (a)) as well as a bifacial cell with an Al finger grid similar to that for the BiCoRE and PERC+ solar cells.**

Phosphorus-doped Czochralski-grown silicon wafers with a resistivity of 6.5Ωcm after final cell processing and an initial thickness of 170µm are employed. The saw damage is removed in potassium hydroxide (KOH), and an RCA cleaning sequence is subsequently performed. The wafers are diffused in a quartz tube furnace using boron tribromide ($BBr_3$). The resulting boron doping has a sheet resistance of around 100Ω/sq.

After removing the BSG in HF, the rear side of the wafer is coated with PECVD $SiN_z$ with a refractive index of 1.9, which acts as a barrier during the texturing of the front side and the subsequent phosphorus diffusion; the sheet resistance is around 130Ω/sq. after cleaning [28]. Next, the phosphorus silicate glass (PSG) and the $SiN_z$ layer are removed in HF. The rear side of the wafer is passivated using a stack of atomic-layer-deposited aluminium oxide (ALD $AlO_x$) and PECVD $SiN_y$ with refractive index $n$ of 2.05. The front side is passivated with PECVD SiNy. The dielectric stack on the rear side is then locally ablated using a pulsed laser source (wavelength = 532nm and pulse length = 10ps), forming line-shaped LCOs. Different LCO widths of 20, 40, 56, 77, 93, 114 and 150µm are used in order to optimize the Al-BSF formation in combination with the Al finger grid design similar to that demonstrated for PERC+ solar cells [11]. The pitch of the LCO lines, however, is kept constant at 1270µm regardless of the LCO width.

The Ag front grid is metallized by means of a dual print process: first the five busbars are printed using a screen and then the fingers are printed using a stencil. The group of cells with an LCO width of 150µm receives a full-area Al screen-print, whereas the other groups with LCO widths between 20µm and 114µm receive a screen-printed Al finger grid with a finger opening width of 100µm. These combinations of LCO widths and Al prints are chosen because in the case of a full-area Al layer, very wide LCO widths result in the deepest Al-BSFs and hence the highest n-PERT BJ efficiencies [14]; in the case of Al fingers, however, it has been demonstrated that much narrower LCO widths yield the deepest Al-BSFs for PERC+ cells [11].

The process sequence is completed by firing the solar cells in a belt furnace. A schematic of the resulting monofacial n-PERT BJ cell is shown in Fig. 1(a).

The $I$–$V$ parameters of the resulting monofacial and bifacial n-PERT BJ solar cells are measured by illuminating the cells from the front side (Ag grid) and contacting the full rear side (Al layer or Al finger grid) with a reflective brass chuck. The results are summarized in Fig. 2 for different LCO widths.

When passing from 114µm-wide LCOs to 40µm-wide LCOs in combination with Al fingers, the conversion efficiency $\eta$ improves from 20.6% to a best value of 21.1% (Fig. 2(a)). The n-PERT BJ cells with an LCO width of 150µm and a full-area Al layer show top efficiencies of up to 21.0%, which is close to the best published value of 21.2% by ISFH [28].

The open-circuit voltage $V_{oc}$

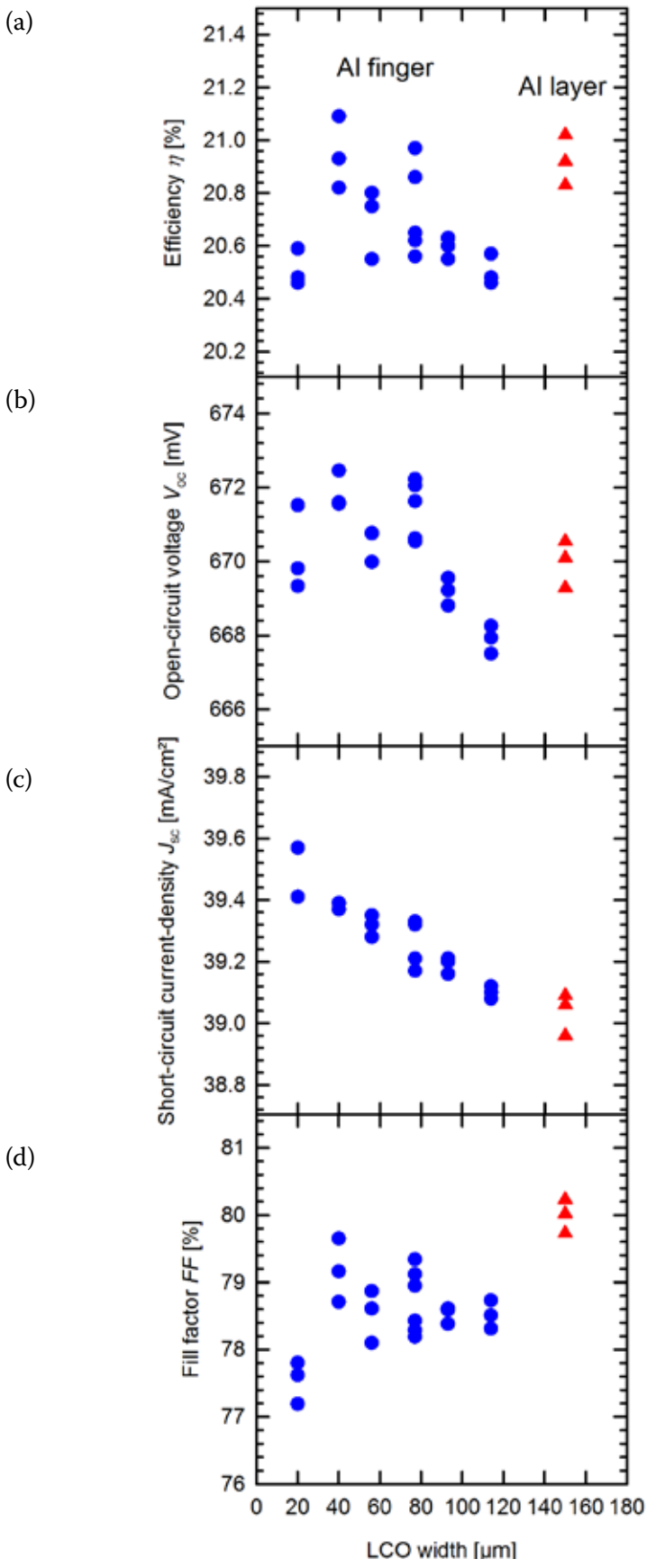


**Figure 2. *I–V* parameters of monofacial and bifacial n-PERT BJ solar cells as a function of LCO width: (a) efficiency $\eta$; (b) open-circuit voltage $V_{oc}$; (c) short-circuit current density $J_{sc}$; (d) fill factor FF. (The cells with LCO widths between 20 and 114µm receive an Al finger grid design, whereas the cells with 150µm LCO widths are screen printed with a full-area Al layer.)**

increases from 668mV for 114µm LCOs to 672mV for 40µm LCOs (Fig. 2(b)). This trend in $V_{oc}$ has been reported for PERC+ cells as well, and has been attributed to the reduced contact-area fraction of the local Al rear contacts with decreased LCO widths while maintaining similar deep Al-BSF depths, thereby reducing the total rear contact recombination of the solar cell [11].

The short-circuit current density $J_{sc}$ increases from 39.1mA/cm² to 39.6mA/cm² when the LCO width is reduced from 114µm to 20µm (Fig. 2(c)). There are two reasons for this: 1) narrower LCO widths cause a slightly higher reflectance in the long-wavelength region, since the area fraction of the local Al contacts with poor reflectance is reduced; and 2) narrower LCOs result in slightly higher internal quantum efficiency (IQE) values at wavelengths above 1000nm, since the lower contact-area fraction leads to reduced contact recombination.

The fill factor FF of the n-PERT BJ cells with an Al finger grid is approximately $1\%_{abs}$ lower than that of the n-PERT BJ cells with a full-area Al-BSF, as shown in Fig. 2(d); this is caused by an increase in series resistance from 0.7Ωcm² for the full-area Al cells to 1.1Ωcm² for the Al finger grid cells. This is surprising, since the full-area contacting brass chuck excludes resistive contributions of the Al finger grid, and also the boron emitter resistance contribution is the same for all cells (because the LCO pitch is the same for all cells). In consequence, all cell types should exhibit very similar series resistances and FF values. A root cause of the lower FF of the n-PERT BJ cells with an Al finger grid could be that these cells might not have been fired at an optimum peak temperature. In this experiment, n-PERT BJ cells with Al fingers and full-area Al layer received a very similar peak firing temperature; the results for PERC+, however, indicated that a slightly lower peak firing temperature is required for cells with an Al finger grid than that for cells with a full-area Al layer [11].

The *I–V* parameters of the best monofacial and bifacial n-PERT BJ cells when illuminated from the front are shown in Table 2 (rows 1 and 2). The *I–V* parameters of the bifacial n-PERT BJ cell are also measured when illuminated from the rear (Al contact) by placing the cell upside down on the *I–V* tester, again using a reflective brass chuck which contacts the full Ag front grid. As shown in Table 2 (row 3),

the rear-side efficiency is 16.5% and therefore much lower than the front-side efficiency of 21.1% for the same cell. Accordingly, the bifaciality, which is equal to the rear efficiency divided by the front efficiency, is 80%. The reduced rear-side efficiency is mainly due to the relatively low $J_{sc}$ of 30.8mA/cm$^2$, which is 8.7mA/cm$^2$ lower than the respective front-side $J_{sc}$.

> "One future improvement opportunity for n-PERT BJ cells is to increase the spacing of the LCO rear contacts, which will allow higher bifacialities than PERC+ solar cells."

For comparison, Table 2 (rows 6 and 7) also shows the front- and rear-side $I$–$V$ parameters of the best bifacial PERC+ solar cells published by Dullweber et al. [8]. Basically, the front and rear $I$–$V$ parameters of the bifacial n-PERT BJ cells are very similar to the respective PERC+ values. In the case of PERC+ cells, the low rear $J_{sc}$ value has been explained [7] by the large Al metallization fraction of 14%, as well as by the fact that the anti-reflective properties of the rear passivation stack have not yet been optimized. Both of these mechanisms also explain the low rear $J_{sc}$ of the n-PERT BJ cells, as the device structure is optically identical to that of the PERC+ cells, including the 14% Al area fraction and the planar rear side. One future improvement opportunity for n-PERT BJ cells is to increase the spacing of the LCO rear contacts that have been optimized for the boron emitter sheet resistance; this will allow higher bifacialities than PERC+ solar cells, where the rear LCO spacing is limited by the wafer bulk spreading resistance.

## BiCoRE solar cells with BSG/SiN$_z$

As a next step, the bifacial n-PERT BJ process is simplified by replacing the $BBr_3$ diffusion and the $AlO_x/SiN_y$ rear passivation by the deposition of a stack of BSG and $SiN_z$. The BSG/$SiN_z$ stack has multiple functions: 1) it serves as a dopant source for boron, which diffuses from the BSG into the silicon wafer during the $POCl_3$ co-diffusion; 2) it protects the rear side of the cell from being textured and phosphorus doped; 3) it remains on the rear side of n-PERT BJ cells as a passivation layer stack and anti-reflection coating (ARC).

In order to assess the emitter and passivation quality of the BSG/$SiN_z$ stack, an RCA clean is performed on n-type Cz test wafers, before depositing a 40nm-thick PECVD BSG layer, capped with a 120nm-thick PECVD $SiN_z$ layer, on both wafer surfaces. The test wafers are then exposed to a $POCl_3$ co-diffusion process, in which prior to the PSG deposition an additional thermal budget is applied in order to drive the boron from the BSG layer into the silicon wafer. Further details about the PECVD deposition parameters of the BSG/$SiN_z$ stack, as well as about the $POCl_3$ co-diffusion, have been published by Lim et al. [29]. Finally, the test wafers are fired in a belt furnace using typical contact-firing parameters.

The quasi-steady state photoconductance (QSSPC) of these samples is measured using an intrinsic carrier concentration of Si of $n_i = 8.6\times10^9$cm$^{-3}$. $J_0$ values of 40fA/cm² are achieved at boron sheet resistances $R_{sheet}$ between 90 and 108Ω/sq. by utilizing the BSG/$SiN_z$ stacks as the diffusion source and surface passivation [30]. In comparison, $BBr_3$-diffused test wafers with $AlO_x/SiN_y$ surface passivation yield $J_0$ values of 14fA/cm² at boron sheet resistances $R_{sheet}$ = 102Ω/sq. Hence, the test wafer

| Cell type | Doping / Passivation | Al area fraction [%] | Illumination side | $\eta$ [%] | $V_{oc}$ [mV] | $J_{sc}$ [mA/cm$^2$] | FF [%] |
|---|---|---|---|---|---|---|---|
| n-PERT BJ | $BBr_3$ / $AlO_x/SiN_y$ | 100 | front | 21.0 | 670 | 39.1 | 80.2 |
| n-PERT BJ (bifacial) | $BBr_3$ / $AlO_x/SiN_y$ | 14 | front | 21.1 | 674 | 39.5 | 79.3 |
| n-PERT BJ (bifacial) | $BBr_3$ / $AlO_x/SiN_y$ | 14 | rear | 16.5 | 669 | 30.8 | 80.0 |
| BiCoRE | $BSG/SiN_z$ | 14 | front | 20.6 | 669 | 39.3 | 78.4 |
| BiCoRE | $BSG/SiN_z$ | 14 | rear | 16.1 | 663 | 30.7 | 79.1 |
| PERC+ | n.a./ $AlO_x/SiN_y$ | 14 | front | 21.5 | 666 | 40.1 | 80.4 |
| PERC+ | n.a./ $AlO_x/SiN_y$ | 14 | rear | 16.6 | 660 | 31.3 | 80.7 |

**Table 2. *I–V* parameters measured under standard testing conditions (STC) of 156mm × 156mm n-PERT BJ and BiCoRE silicon solar cells. For comparison, the best PERC+ solar cell results published by Dullweber et al. [8] are also shown.**

results indicate that the $BSG/SiN_z$ stack is well suited to functioning as a dopant source and passivation layer, resulting in similar sheet resistances to those for the $BBr_3$-diffused samples and slightly higher $J_0$ values, which are subject to future improvements.

The $BSG/SiN_z$ stack is now implemented in BiCoRE solar cells; the detailed process flow is shown in Table 1 (column 2). The same 156mm × 156mm n-type Cz wafers as for the n-PERT BJ solar cells are employed. After initial wafer cleaning, the PECVD $BSG/SiN_z$ stack is deposited on the wafer rear surface, followed by an alkaline texturing and a $POCl_3$ co-diffusion. Because of the $SiN_z$ rear capping layer, only the wafer front side is textured and phosphorus doped. The PSG on the wafer front side is removed by a short HF dip; this, however, does not remove the $BSG/SiN_z$ stack on the wafer rear side. A PECVD $SiN_y$ anti-reflection coating is then deposited on the wafer front side. The rear contacts are formed by laser ablation using the optimum LCO width of 40µm and the same pitch as for the bifacial n-PERT BJ cells. The Ag front contacts are dual printed, and the Al rear finger grid is screen printed using a finger opening of 100µm by utilizing the same processes as for the bifacial n-PERT BJ cells (as described in the previous section).

A schematic of the resulting BiCoRE solar cell is shown in Fig. 1(b). For comparison, Table 1 (column 3) and Fig. 1(c) also show the process sequence and schematic of a p-type PERC+ solar cell. The process flow for the BiCoRE cell is intentionally designed to be as close as possible to that for PERC+ solar cells in order to allow PERC cell manufacturers to change their production process to that for BiCoRE cells with almost no additional tool investment.

The *I–V* parameters of the BiCoRE solar cells are measured using the same measurement set-up as described earlier for n-PERT BJ solar cells; the results are summarized in Table 2 for the best BiCoRE solar cell. The average *I–V* parameters of four identically processed BiCoRE cells are also given in brackets in the following text. When illuminated from the front (row 4 in Table 2), the best BiCoRE solar cell demonstrates a conversion efficiency $\eta$ of 20.6% (average 20.3%), a $V_{oc}$ of 669mV (average 670mV), a $J_{sc}$ of 39.3mA/cm$^2$ (average 39.3mA/cm$^2$) and a FF of 78.4% (average 77.1%). These values are fairly close to the *I–V* parameters in Table 2 (row 2) of the bifacial n-PERT BJ cell with $BBr_3$ diffusion and $AlO_x/SiN_y$ rear passivation.

The slightly lower efficiency of the BiCoRE cell can be attributed to a $POCl_3$ co-diffusion that has not yet been optimized, resulting in higher sheet resistances of the front-surface field, causing higher contact resistances of the Ag pastes and hence 0.9%$_{abs}$ smaller FF values. The 5mV lower $V_{oc}$ of the BiCoRE cell is partly due to the 26fA/cm$^2$ higher $J_0$ of the PECVD $BSG/SiN_z$ co-diffused and passivated rear emitter, compared with the $BBr_3$-diffused and $AlO_x/SiN_y$-passivated n-PERT BJ cell.

The BiCoRE solar cell stems from the first batch of cells created using this novel process sequence. The authors are confident that with further optimization of the $BSG/SiN_z$ stack and the $POCl_3$ co-diffusion, it will be possible to produce BiCoRE cells with *I–V* parameters comparable to those of n-PERT BJ and PERC+ solar cells.

## Conclusions

A novel industrial solar cell design has been introduced, namely BiCoRE. A key feature of this cell is a $BSG/SiN_z$ stack on the rear wafer side, which has three functions: 1) a protection layer against texturing and $POCl_3$ diffusion; 2) a boron dopant source during the $POCl_3$ co-diffusion; and 3) a passivation layer. Bifaciality is realized by utilizing LCO and screen printing an Al finger grid on the rear, similarly to the recently introduced PERC+ solar cells.

> "With further optimizations of the $BSG/SiN_z$ stack and the $POCl_3$ co-diffusion, it is expected that BiCoRE cells will yield efficiencies that are comparable to those of today's PERC+ solar cells."

When the LCO widths were varied it was found that, in the case of Al fingers, narrow LCO widths of 40µm result in Al-BSFs with depths of up to 8.5µm and in conversion efficiencies of up to 21.1% for n-PERT BJ reference cells. The multifunctional $BSG/SiN_z$ stack demonstrates emitter saturation current densities of 40fA/cm$^2$ on test wafers, enabling conversion efficiencies of up to 20.6% for BiCoRE solar cells. When illuminated from the rear side, the BiCoRE cells exhibit conversion efficiencies of up to 16.1%, which corresponds to a bifaciality of 78%.

With further optimizations of the $BSG/SiN_z$ stack and the $POCl_3$ co-diffusion, it is expected that BiCoRE cells, which use LID-stable

n-type wafers, will yield even higher efficiencies – indeed, efficiencies that are comparable to those of today's PERC+ solar cells. The BiCoRE cell design could therefore become an attractive option for PERC solar cell manufacturers in changing their production to a bifacial, LID-stable cell concept with only a minimal conversion investment, which would mainly involve changing the PECVD $AlO_x/SiN_y$ deposition to a $BSG/SiN_z$ deposition process.


## Acknowledgements

We thank our colleagues M. Berger for solar cell processing, F. Heinemeyer for SEM measurements, and D. Hinken for support in the IQE analysis. This work was funded by the German Federal Ministry for Economic Affairs and Energy under Contract No. 0325880A (PERC 2.0).


## References


[1] Fischer, G. et al. 2015, *Energy Procedia*, Vol. 77, pp. 515–519.

[2] SolarWorld 2015, "SolarWorld expands production in Arnstadt", Press Release (Mar) [http://www.solarworld.de/en/group/investor-relations/news-announcements/corporate-news/single-ansicht/article/solarworld-expands-production-in-arnstadt].

[3] Hanwha Q CELLS 2015, "Hanwha Q Cells announces over 1.5 GW solar module supply agreement to power NextEra Energy Resources' continued solar investments in the U.S.", Press Release (Apr) [http://investors.hanwha-qcells.com/releasedetail.cfm?ReleaseID=907243].

[4] Verlinden, P.J. et al. 2014, *Proc. 6th WCPEC*, Kyoto, Japan.

[5] Trina Solar 2015, "Trina Solar starts PERC technology volume production", Press Release (Jan) [http://www.pv-tech.org/news/trina_solar_starts_perc_technology_volume_production].

[6] SEMI PV Group Europe 2015, "International technology roadmap for photovoltaic (ITRPV): 2014 results", 6th edn (Apr.) [http://www.itrpv.net/Reports/Downloads/].

[7] Dullweber, T. et al. 2015, *Prog. Photovoltaics Res. Appl.*, DOI: 10.1002/pip.2712.

[8] Dullweber, T. et al. 2015, *Proc. 31st EU PVSEC*, Hamburg, Germany, pp. 341–350.

[9] Guo, S., Walsh, T.M. & Peters, M. 2013, *Energy*, Vol. 61, pp. 447–454.

[10] Janssen, G.J.M. et al. 2015, *Energy Procedia*, Vol. 77, pp. 364–373.

[11] Kranz, C. et al. 2016, *IEEE J. Photovolt.*, Vol. 6, pp. 830–836.

[12] Mertens, V. et al. 2013, *Proc. 28th EU PVSEC*, Paris, France, pp. 714–717.

[13] Aleman, M. et al. 2013, *Proc. 28th EU PVSEC*, Paris, France, pp. 731–735.

[14] Lim, B. et al. 2014, *Proc. 29th EU PVSEC*, Amsterdam, The Netherlands, pp. 661–665.

[15] Wang, W. et al. 2015, *IEEE J. Photovolt.*, Vol. 5, pp. 1245–1249.

[16] Gassenbauer, Y. et al. 2013, *IEEE J. Photovolt.*, Vol. 3, pp. 125–130.

[17] Dullweber, T. 2013 et al. 2013, *Proc. 39th IEEE PVSC*, Tampa, Florida, USA, pp. 3074–3078.

[18] Walter, D.C. et al. 2014, *Appl. Phys. Lett.*, Vol. 104, pp. 042111/1–4.

[19] Wilking, S. et al. 2014, *Sol. Energy Mater. Sol. Cells*, Vol. 131, pp. 2–8.

[20] Cabal, R. et al. 2009, *Proc. 24th EU PVSEC*, Hamburg, Germany, pp. 1605–1608.

[21] Rothhardt, P. et al. 2014, *Proc. 29th EU PVSEC*, Amsterdam, The Netherlands, pp. 653–655.

[22] Frey, A. et al. 2014, *Proc. 29th EU PVSEC*, Amsterdam, The Netherlands, pp. 656–660.

[23] Wehmeier, N. et al. 2013, *Proc. 28th EU PVSEC*, Paris, France, pp. 1980–1984.

[24] Wehmeier, N. et al. 2016, *physica status solidi (RRL)*, Vol. 10, pp. 148–152 (2016).

[25] Engelhardt, J. et al. 2015, *Appl. Phys. Lett.*, Vol. 107, p. 042102.

[26] Cabal, R. et al. 2016, *Proc. 6th SiliconPV*, Chambéry, France [to be published in *Energy Procedia*].

[27] Dullweber, T. et al. 2016, *physica status solidi (a)*, Vol. 1–7, DOI: 10.1002/pssa.201600346.

[28] Wehmeieri, N. et al. 2016, *Proc. 32nd EU PVSEC*, Munich, Germany, pp. 443–446.

[29] Lim, B. et al. 2016, *IEEE J. Photovolt.*, Vol. 6, pp. 447–453.

[30] Wehmeier, N. et al. 2016, *Sol. Energy Mater. Sol. Cells*, DOI:10.1016/j.solmat.2016.05.054.


## About the Authors

**Dr. Thorsten Dullweber** leads the industrial solar cells R&D group at ISFH. His research work focuses on high-efficiency, industrial-type, PERC silicon solar cells and on ultra-fine-line, screen-printed, Ag front contacts. Before joining ISFH in 2009, he worked for nine years as a project leader in the microelectronics industry at Siemens AG and then at Infineon Technologies AG.

**Nadine Wehmeier** studied physics at the University of Münster, Germany, and received her M.Sc. in 2011 for her work on silicon multilayer structures for thermoelectric applications. She has been working towards a Ph.D. with ISFH since 2012, where she is researching plasma-enhanced chemical vapour deposition layers as diffusion sources and co-diffusion processes.

**Anja Nowack** completed her studies in process engineering at the University of Applied Sciences Nordhausen. For her Diploma thesis she carried out research into renewable energies with regard to optimizing the production of biogas. Since 2010 she has been working at ISFH as a degreed engineer (Dipl. Ing. (FH)), initially on topics involving macroporous silicon and then on PECVD BSG layers.

**Till Brendemühl** received his Diploma degree in engineering physics from the University of Applied Science in Emden, Germany. Since 2005 he has been with ISFH, where he initially worked on laser processes, and then later became a project leader with a focus on back-contact, high-efficiency solar cells. He is currently working on screen-printed, n-PERT solar cells in the photovoltaic future technologies group.

**Rolf Brendel** received a Ph.D. in materials science in 1992 from the University of Erlangen, Germany, for his work on infrared spectroscopy. After a research post at the Max Planck Institute for Solid State Research in Stuttgart, he was appointed head of the thermosensorics and photovoltaics division at the Bavarian Center for Applied Energy Research in 1997. In 2004 he joined the Institute of Solid State Physics at the Leibniz University of Hanover as a full professor, and became director of ISFH.

## Enquiries


Dr. Thorsten Dullweber
Institute for Solar Energy Research Hamelin (ISFH)
Am Ohrberg 1
D-31860 Emmerthal
Germany